

12

AFGL-TR-81-0325

INVERSION OF SPIRE NO DATA

LEVEL II

A.S. Zachor
R.D. Sharma
R.M. Nadile
A.T. Stair, Jr.

Atmospheric Radiation Consultants, Inc.
59 High Street
Acton, Massachusetts 01720

12 36

Scientific Report No. 2

20 August 1981

Approved for public release; distribution unlimited

AD A108866

DTIC FILE COPY

AIR FORCE GEOPHYSICS LABORATORY
AIR FORCE SYSTEMS COMMAND
UNITED STATES AIR FORCE
HANSCOM AFB, MASSACHUSETTS 01731

DTIC
ELECTE
DEC 28 1981

061150

Boston
coll. D

8112 28066

2

Unclassified

SECURITY CLASSIFICATION OF THIS PAGE (When Data Entered)

REPORT DOCUMENTATION PAGE		READ INSTRUCTIONS BEFORE COMPLETING FORM
1. REPORT NUMBER AFGL-TR-81-0325	2. GOVT ACCESSION NO. AD A108866	3. RECIPIENT'S CATALOG NUMBER
4. TITLE (and Subtitle) INVERSION OF SPIRE NO DATA		5. TYPE OF REPORT & PERIOD COVERED Scientific Report No. 2
		6. PERFORMING ORG. REPORT NUMBER
7. AUTHOR(s) A. S. Zachor R. D. Sharma* R. M. Nadile* A. T. Stair, Jr.*		8. CONTRACT OR GRANT NUMBER(s) F19628-79-C-0139 Boston College Subcontract No. 922-22
9. PERFORMING ORGANIZATION NAME AND ADDRESS Atmospheric Radiation Consultants, Inc. 59 High Street Acton, Massachusetts 01720		10. PROGRAM ELEMENT, PROJECT, TASK AREA & WORK UNIT NUMBERS 62101F 767010AF
11. CONTROLLING OFFICE NAME AND ADDRESS Air Force Geophysics Laboratory (OPR) Hanscom AFB, MA 01731 Contract Monitor: John A. Sandock/OPR-1		12. REPORT DATE 20 August 1981
		13. NUMBER OF PAGES 35
14. MONITORING AGENCY NAME & ADDRESS (if different from Controlling Office)		15. SECURITY CLASS. (of this report) Unclassified
		15a. DECLASSIFICATION/DOWNGRADING SCHEDULE
16. DISTRIBUTION STATEMENT (of this Report) Approved for public release; distribution unlimited.		
17. DISTRIBUTION STATEMENT (of the abstract entered in Block 20, if different from Report)		
18. SUPPLEMENTARY NOTES * AIR FORCE GEOPHYSICS LABORATORY, HANSCOM AFB, MA 01731		
19. KEY WORDS (Continue on reverse side if necessary and identify by block number.) Limb inversion, inversion algorithm, spectrally resolved data, optically thin, nitric oxide (NO), SPIRE, CIRRS, excited NO density retrieval, temperature retrieval, 5.3 μ m band, cooling rate, de-excitation rate constant		
20. ABSTRACT (Continue on reverse side if necessary and identify by block number.) An algorithm was developed to invert spectrally resolved Earth limb radiance profiles. It is applicable in the nonequilibrium altitude regime for species/tangent heights that correspond to the optically thin condition. It was used to infer vertical distributions of temperature and excited NO density from data measured by SPIRE (the Spectral Infrared Rocket Experiment) in the NO fundamental band near 5.3 μ m. The solution for excited NO density was used to compute atmospheric radiative cooling rates for the 5.3 μ m band and the de-excitation rate constant k_0 for the reaction $NO^+ + O \rightarrow NO + O$. The results are in good agreement		

DD FORM 1 JAN 73 1473

EDITION OF 1 NOV 65 IS OBSOLETE

Unclassified

SECURITY CLASSIFICATION OF THIS PAGE (When Data Entered)

[Handwritten signatures and initials]

Unclassified

SECURITY CLASSIFICATION OF THIS PAGE(When Data Entered)

with previously published values.

Unclassified

SECURITY CLASSIFICATION OF THIS PAGE(When Data Entered)

TABLE OF CONTENTS

	<u>PAGE</u>
SECTION 1 INTRODUCTION AND SUMMARY	1
SECTION 2 INVERSION ALGORITHMS	3
2.1 Relaxation Method	6
2.2 Analytical Solutions for a Special Case	8
2.3 Inversion using Fourier Transforms.	9
SECTION 3 LIMB RADIANCE DATA AND INVERSION RESULTS	10
3.1 Results for $n^*(H)$	13
3.2 Results for $T(H)$	16
SECTION 4 INTERPRETATION OF RESULTS.	22
REFERENCES	26
APPENDIX A	28
APPENDIX B	30

Accession For	
NTIS GRA&I	<input checked="" type="checkbox"/>
DTIC TAB	<input type="checkbox"/>
Unannounced	<input type="checkbox"/>
Justification	
By _____	
Distribution/	
Availability Codes	
Dist	Avail and/or Special
A	

SECTION 1
INTRODUCTION AND SUMMARY

An objective of the CIRRIS Program* is to obtain measurements that

- (a) define the Earth's limb as an IR spectral background, and
- (b) provide information on photochemical processes in both the quiescent and disturbed atmosphere.

Interpretation of the limb data in terms of atmospheric photochemistry will include mathematical inversions of the data, i.e., transformation of the measured limb radiance profiles into vertical distributions of concentration and temperature.

CIRRIS will obtain spectrally resolved Earth limb radiance profiles up to several hundred kilometers tangent height. Quantities that can be inferred for the nonequilibrium atmosphere ($H \approx 70$ km) through an inversion of the data include ground state and excited state species concentration and rotational temperature. However, limb inversion techniques applicable to spectrally resolved data and to the non-LTE altitude regime have not been studied extensively. These differ significantly from limb inversion methods developed for the lower atmosphere (e.g., Gille and House, 1971).

The purpose of the present study was to develop an algorithm applicable to a special nonequilibrium case, namely, the recovery of the distribution of excited nitric oxide and kinetic temperature above 100 kilometers from limb spectral radiances measured in the fundamental ($\Delta v = 1$) band at $5.3 \mu\text{m}$. This is a special case because ground state NO is optically thin for tangent paths above ~ 100 km for the fundamental band. The study results provide a starting point for development of algorithms applicable to the non-optically-thin, nonequilibrium case, which will be required in analyzing CIRRIS data.

The developed algorithm was applied to NO spectral radiance profiles measured by SPIRE (Spectral Infrared Rocket Experiment). The excited NO

* CIRRIS is an acronym for Cryogenic InfraRed Radiance Instrumentation for Shuttle. The CIRRIS Program is described by Ahmadjian, *et al* (1980).

densities were used to compute atmospheric radiative cooling rates for the 5.3 μm band, and the de-excitation rate constant k_0 for the reaction $\text{NO}^* + \text{O} \rightarrow \text{NO} + \text{O}$. These results are discussed in Sections 3 and 4. Section 2 describes the inversion algorithms. The SPIRE instrument and data it obtained are described by Nadile *et al* (1977) and Stair *et al* (1981).

The solution for NO excited density and the computed cooling rates and de-excitation rate constant are in good agreement with other published measurements and models. The solution for temperature is limited by noise in the SPIRE spectral data.

SECTION 2
INVERSION ALGORITHMS

The geometry of the limb observations is shown in Fig. 1a. The *band* radiance at the sensor due to excited NO molecules in path segment dz is

$$dN(H_T) = (A/4\pi) dz n^*(z) , \quad (1)$$

where H_T is the tangent height of the observation, $n^*(z)$ is the density of the excited molecules at altitude $H(H_T, z)$ and A is the Einstein A-coefficient for the band (NO fundamental). We have assumed that reabsorption by ground state NO over the tangent path can be neglected. The band radiance due to the entire path can be expressed as an integral over altitude:

$$N(H_T) = \frac{2A}{4\pi} \int_{H_T}^{\infty} dH \frac{\partial z(H, H_T)}{\partial H} n^*(H) . \quad (2)$$

A form suitable for numerical evaluation or inversion is

$$N(H_j) \equiv N_j = (2A/4\pi) \sum_{i=j}^I \Delta_{i-j+1, j} n_i^* , \quad (3a)$$

where the Δ_{ij} are distances (Δz 's) defined in Fig. 1b. Given a limb profile of the band radiance (set of measurements N_j), one can invert Eq. (3a) to find a set of values n_i^* that approximates $n^*(H)$. The set N_j is obtained by integrating the SPIRE limb radiance spectral data over the NO fundamental band.

Equation (3a) will give a good approximation to the *observed* limb radiance profile if n^* does not vary appreciably over the vertical distance ΔH resolved by the sensor; note that ΔH determines the weights Δ_{ij} . If the variation is appreciable, a smaller ΔH should be used in evaluating Eq. (3a), and the result should be convolved with a function representing the sensor's spatial response in the vertical.

The limb profile of *spectral* radiance measured by a device like the SPIRE CVF spectrometer can be expressed in the form

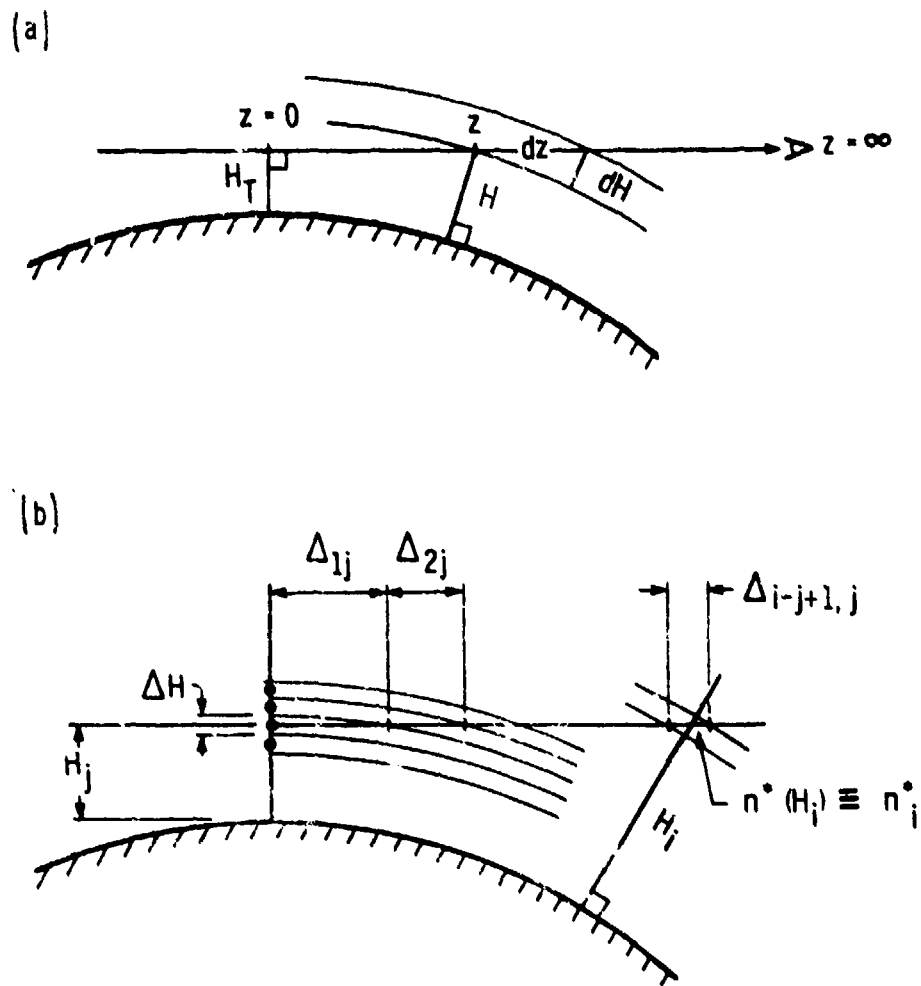


Figure 1. The geometry of the limb inversions.
 Part b defines the weights Δ_{ij} appearing in Eq. (3a).

$$N(H_j, \lambda_k) \equiv N_{jk} = (2A/4\pi) \sum_{i=j}^I \Delta_{i-j+1, j} n_{ik}^{**}, \quad (3b)$$

where

$$n_{ik}^{**} = n_i^* R_{ik} \quad (4)$$

and

$$R[T(H_i), \lambda_k] \equiv R_{ik} = \sum_{\ell} S_{\ell}[T(H_i)] C(\lambda_{\ell}, \lambda_k), \quad (5)$$

where λ_{ℓ} denotes the centers of the rotational lines comprising the band, S_{ℓ} are the line intensities (determined by the NO rotational temperature at altitude H_i), and $C(\lambda_{\ell}, \lambda_k)$ is the spectral response of the instrument at wavelength λ_k due to a line (unit impulse) at $\lambda = \lambda_{\ell}$. The response function C and line intensities S_{ℓ} are normalized such that

$$\int_0^{\infty} R d\lambda = 1 \quad (6)$$

Thus, Eqs. (3b), (4) and (5) merely replace the band source function A of Eq. (3a) by the spectral source function AR , which depends on rotational temperature. Evaluation of the normalized apparent spectral emission R is simplified by the fact that the Doppler broadened lines are very narrow compared to the response function C ; they can be treated as delta functions. However, the instrument response function C (which is dominated by the spectral response of the CVF) depends on both λ_{ℓ} and λ_k , not on $\lambda_k - \lambda_{\ell}$; i.e., R cannot be represented as the convolution of a single function with a series of impulses.

Given a data set N_{jk} versus j for fixed k (limb profile of spectral radiance at fixed spectrometer setting λ_k), one can invert Eq. (3b) in the same manner as Eq. (3a) to obtain n_{ik}^{**} versus i . Then R_{ik} can be found from Eq. (4), using the solution n_i^* obtained by inverting the band radiance profile. By repeating the process at other wavelengths one obtains R_{ik} versus k and i , i.e., the normalized spectral distribution R versus λ for different altitudes. Finally, each of these recovered spectral distributions can be compared to ones computed from Eq. (5) for various rotational

temperatures T, to determine the temperature that gives the best agreement. The result is a solution for the vertical distribution of the NO rotational temperature (which is the same as the kinetic temperature, except at altitudes greater than ~160 km).

Note that this procedure for recovering rotational temperature is not restricted to the case of low spectral resolution. However, if the sensor can resolve individual lines, it may be desirable to use integrated line radiances rather than spectral radiances, and to redefine N_{jk} and R_{ik} accordingly.* The SPIRE data used to recover the temperature profile consisted of 10 spectrum values with wavelength spacing between 0.05 μm and 0. μm .

Equations (3a) and (3b) were inverted using a so-called direct nonlinear technique. The method starts with an initial guess for the solution n_i^* or n_{ik}^{**} , and uses the equations to compute the corresponding limb profile N_j or N_{jk} . Ratios between the measured and computed profile values are used to relax the initial guess. The process is iterated until the rms difference between computed and measured limb radiances is smaller than some preassigned value, which might be the system noise. Solutions obtained by such a method are generally non-unique, and the number of values comprising the solution may exceed the number of observations. The efficiency of the inversion procedure and, to some extent, the quality of the solution, depends on the particular relaxation method employed.

2.1 Relaxation Method

Equation sets (3a) and (3b) evaluated in the nth iteration have the form

$$\begin{aligned}
 o_1^{(n)} &= w_{11}s_1^{(n)} + w_{21}s_2^{(n)} + w_{31}s_3^{(n)} + \dots \\
 o_2^{(n)} &= \quad \quad \quad w_{12}s_2^{(n)} + w_{22}s_3^{(n)} + \dots \\
 o_3^{(n)} &= \quad \quad \quad \quad \quad w_{13}s_3^{(n)} + \dots \\
 &\vdots
 \end{aligned} \tag{7}$$

*The choice of spectral resolution for a limb inversion sensor involves many issues, including available signal-to-noise and the possibility of spectral interferences from other atmospheric species. Low to moderate resolution may be optimum in some circumstances.

where the $s_i^{(n)}$ represent the iterated guess for the solution profile, w_{mj} are the weights $(2A/4\pi)\Delta_{mj}$, and $o_j^{(n)}$ are the corresponding computed limb radiances or spectral radiances. Let $o_j^{(o)}$ denote the limb observations. The relaxation procedure used in the present study can be described as a scaling and averaging operation:

- a.) For the j th tangent height (j th row of Eq. (7)), calculate the quantity $(o_j^{(o)}/o_j^{(n)})^K$. Multiply each $s_i^{(n)}$ of the j th row by this quantity.
- b.) After scaling each row in this manner, obtain $s_i^{(n+1)}$ as the sum of the elements of column i divided by the sum of the weights in column i . The $s_i^{(n+1)}$ are the new solution, or final solution if the convergence criterion is satisfied.

This is the scaling/averaging operation proposed by Halem and Chow (1976) for the nadir inversion problem, except that in the present case the information channels correspond to tangent height rather than spectral subbands. The formal relaxation equation for the limb geometry is

$$s_i^{(n+1)} = s_i^{(n)} \frac{\sum_{j=1}^{i'} \Delta_{i-j+1,j} \left(o_j^{(o)} / o_j^{(n)} \right)^K}{\sum_{j=1}^{i'} \Delta_{i-j+1,j}} ; \quad (8)$$

$$i = 1, 2, \dots, I; \quad J = \text{number of } o_j^{(o)}; \quad i' = \min(i, J) .$$

The optimum value for the exponent K is determined by experimentation. The value $K \approx 1.5$ was found to yield the maximum rate of convergence in the inversions of SPIRE NO data.

The measured limb radiance profile has upper and lower bounds on tangent height corresponding to subscripts $j = 1$ and J , respectively. The upper bound is determined by the instrument sensitivity (noise) or the upper limit of the spatial scan. It is for this reason that the limit i' in the summations in Eq. (8) is equal to the smaller of the indices i and J . Note that the number of solution values I can be greater than the number of observations J .

The weights Δ_{mj} in Eqs. (3a), (3b) and (8) are given by (see Fig. 1b)

$$\Delta_{mj} = z_{mj} - z_{m-1,j} \quad (9)$$

where

$$z_{0j} = 0, \quad (10)$$

$$z_{mj} = \left\{ [R + H_j + (m-1 + 1/2)\Delta H]^2 - (R + H_j)^2 \right\}^{1/2}; \quad m = 1, 2, \dots,$$

and R is the Earth's radius. Note that z_{mj} can be approximated by

$$z_{mj} \approx [\Delta H(R + \bar{H}_T)]^{1/2} (2m-1)^{1/2} \equiv z_m \quad (11)$$

where \bar{H}_T is an average tangent height. The maximum relative error in Δ_{mj} due to this approximation is about one percent over the range of altitudes involved in the NO inversions. Thus, the weights Δ_{mj} which appear in both numerator and denominator of the relaxation formula, Eq. (8), can be replaced by the much simpler quantity w_m :

$$w_1 = 1$$

$$w_m = (2m-1)^{1/2} - (2m-3)^{1/2}; \quad m = 2, 3, \dots, \quad (12)$$

This approximation was used for relaxing the guess solution. The exact equations (9) and (10) were used in evaluating the limb radiances for the iterated guess.

2.2 Analytical Solutions for a Special Case

Studies dealing with the reaction chemistry and thermal budget of the upper atmosphere, such as Gordiets, *et al* (1980) and Kockarts (1980), have derived or made use of models in which the density of excited NO varies nearly exponentially with altitude above $H \approx 150$ or 200 km. It can be shown that the function $N(H_j)$ is approximately proportional to $n^*(H)$ when the latter is exponential; i.e., the limb radiance profile is approximately an exponential

with the same decay constant. More generally, the contribution of an arbitrary atmospheric layer (H_1, H_2) to the limb radiance at some tangent height $H_T \leq H_1$ can be expressed in an approximate closed form; that is, in terms of an exponential and the error function. The analytical solutions are given in Appendix A.

The SPIRE integrated limb spectra are roughly exponential at the higher limb tangent heights ($H_T \gtrsim 175$ km) if the noise is averaged; the noise becomes significant above 175 km. SPIRE data for the high altitudes and any other measurements that exhibit the exponential behavior can be "instantly inverted" using the analytical solution. The more general solution given in Appendix A is useful in establishing practical limits for the integrations required in the inversions.

2.3 Inversion using Fourier Transforms

The geometric approximation used to simplify the relaxation equation and to obtain the analytical solutions for an exponential limb radiance profile can also be used to show that Eqs. (3a) and (3b) can be expressed approximately as convolutions. This means that the inversion (for the optically thin case) can, in principle, be performed as a deconvolution, that is, by Fourier transform, multiplication and inverse Fourier transform operations. The method is described in Appendix B. It is possible that the method, implemented via the FFT algorithm, is more efficient than the direct nonlinear method described above. However, we have not tested the method. Unlike the direct nonlinear method it cannot be adapted to the non-optically-thin case.

SECTION 3 LIMB RADIANCE DATA AND INVERSION RESULTS

It was determined that a reasonable altitude increment ΔH for the numerical integrations (see Fig. 1b) is 2.5 km. The upper part of Fig. 2 shows an approximation to the weighting function $\partial z/\partial H$ and the corresponding numerical weights evaluated for $\Delta H = 2.5$ km. The weighting function in the figure is $\partial z/\partial H = \text{const.} \times (H-H_T)^{-1/2}$ (see Appendix A), and the numerical weights are the integral of this approximation over the intervals $(H_T, H_T + 0.5 \Delta H)$, $(H_T + 0.5 \Delta H, H_T + 1.5 \Delta H)$, $(H_T + 1.5 \Delta H, H_T + 2.5 \Delta H)$, ...; i.e., the latter are given by Eq. (12). The two dashed curves show the maximum relative variation of excited NO density with altitude in a model used by Kockarts (1980). It is seen that an integration mesh size of 2.5 km is adequate for computing the limb profile due to excited NO, if the actual gradients are no larger than those of Kockarts' model. The value used for $A \equiv A_{v \rightarrow v'} = A_{0+1}$, the thermally averaged Einstein emission coefficient for the $v' = 1$ transition of the NO fundamental, is 10.78 sec^{-1} , after Billingsley (1975).

The SPIRE instrument resolved appropriately 5 km at the tangent height, for tangent heights between 120 and 160 km. Therefore, it was necessary to degrade the spatial resolution of the limb profiles computed by Eqs. (3a) and (3b) before comparing them to the SPIRE measured profiles. The procedure consisted of convolving the N_j with the three-point numerical comb (1/4, 1/2, 1/4), which represents the sensor IFOV as a rectangular (boxcar) function of width 5 km. The effective numerical weighting function for the SPIRE observations is shown in the lower part of Fig. 2. This was obtained by convolving the weights in the upper part of the figure with the numerical IFOV comb.

Figure 3 shows several band radiance limb profiles obtained by integrating the SPIRE spectral data over the NO 5.3 μm band. Scans 4 and 9 observed the limb in daylight. In scan 8, tangent heights below ~ 130 km are in darkness; the relatively high radiance levels between 90 and 120 km suggest that this scan may have observed a weak aurora (see Stair *et al.* 1981). The spacing of the data in tangent height is approximately four to eight km.

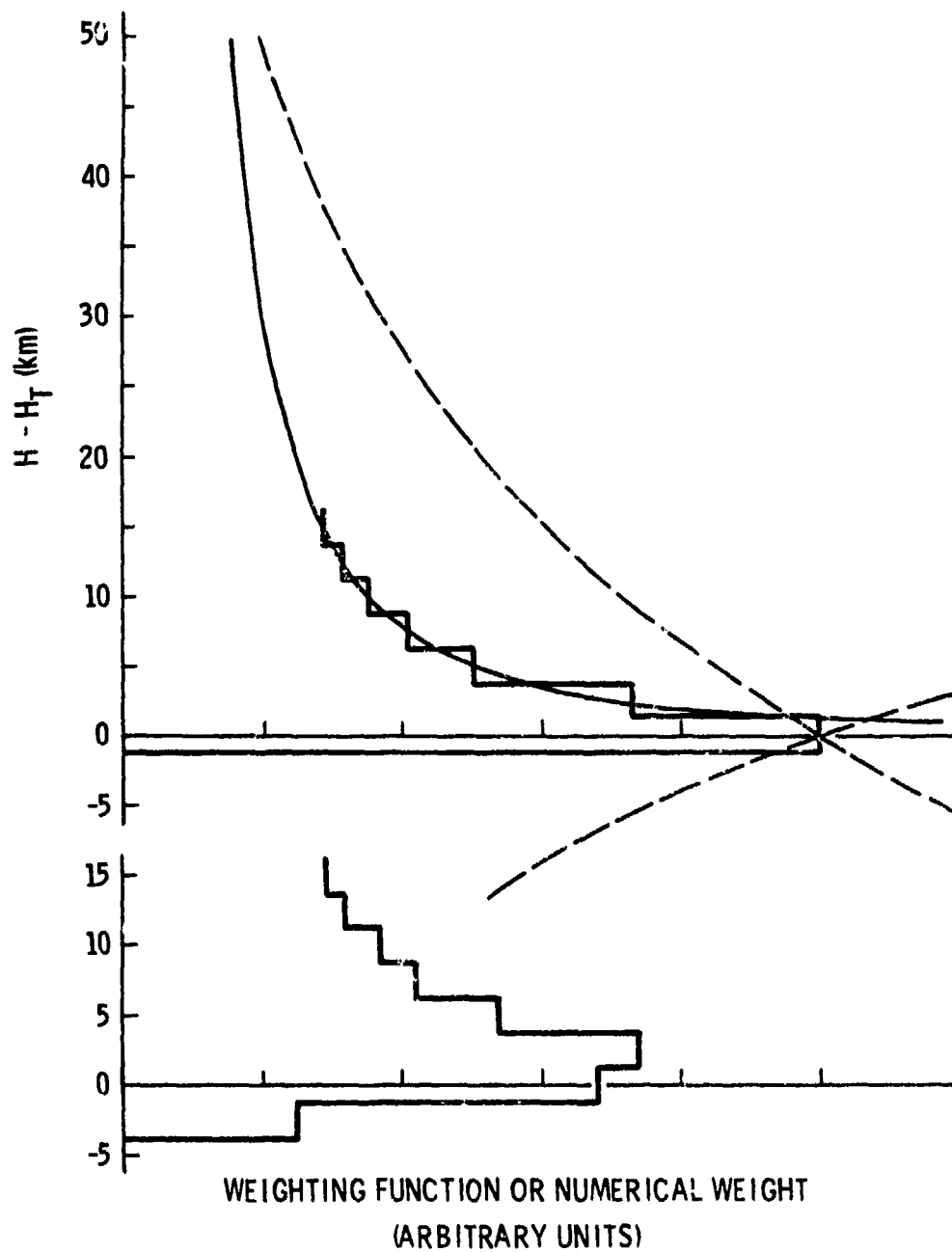


Figure 2. Approximate weighting function for optically-thin limb inversion, and the corresponding numerical weights for the integration mesh size $\Delta H = 2.5$ km.

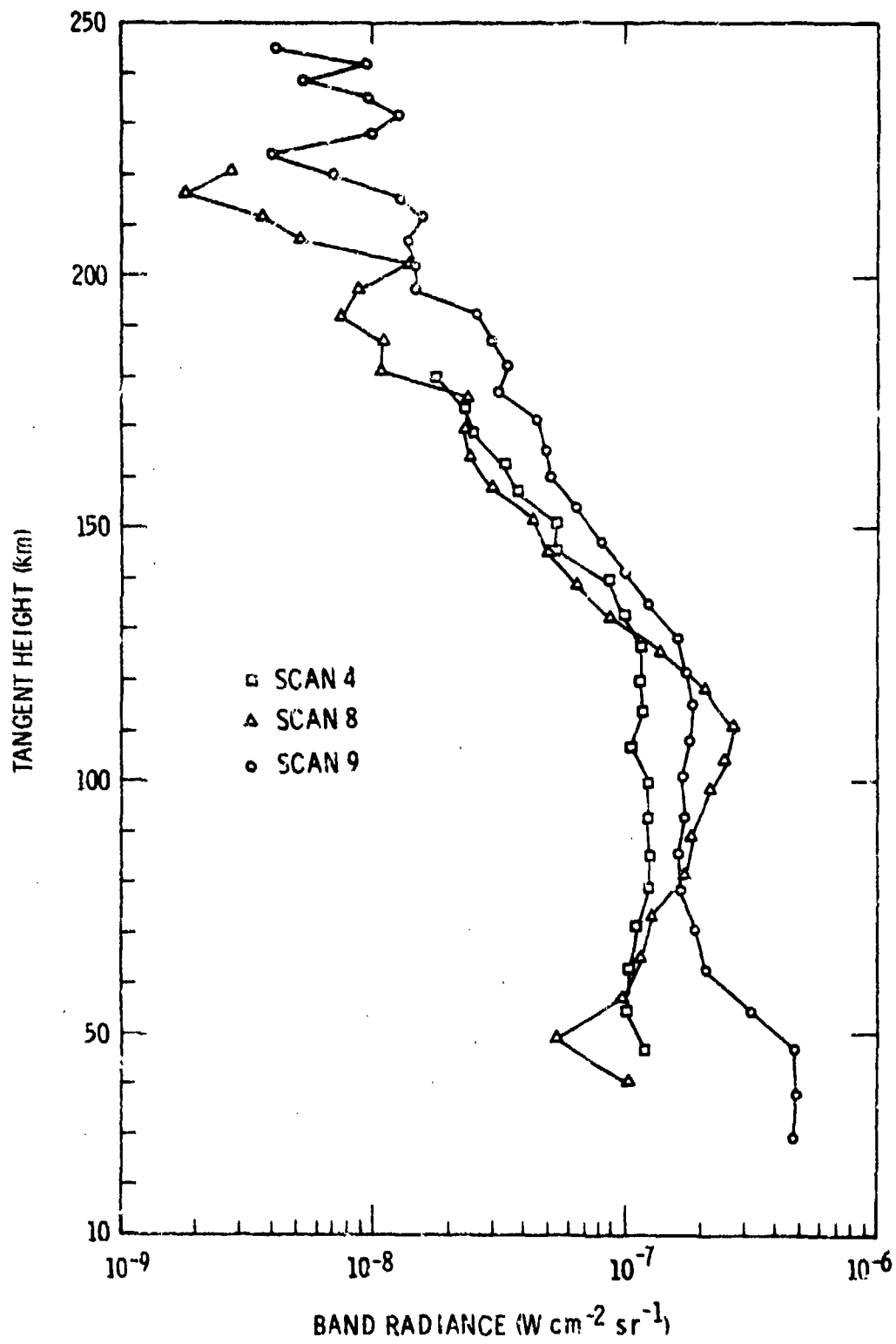


Figure 3. Limb radiance profiles obtained by SPIRE for the NG fundamental band (5.08-5.64 μm).

The SPIRE noise equivalent band radiance is approximately $2 \times 10^{-8} \text{ W cm}^{-2} \text{ sr}^{-1}$ in the NO band. The noise is evident at the higher tangent heights.

The continuous curve in Fig. 4 is the spectral radiance measured by SPIRE at tangent height $H_T = 122 \text{ km}$ during scan 9. The nonzero baseline is an artifact caused by saturation of the detector at an earlier time in the CVF spectral scan sequence. The baseline effect is greatest at the lower tangent heights, and becomes negligible when $H_T \approx 130 \text{ km}$. The baseline was assumed to be linear with wavelength and was estimated from spectral radiances near the band edges; it was removed before the data was inverted. Data for $H_T < 100 \text{ km}$ was not used because it is not clear that the correction method is valid when the baseline spectral radiance is large. Figure 3 shows *uncorrected* profiles. The dashed curve in Fig. 4 is described in a later section.

3.1 Results for $n^*(H)$

The SPIRE data for scan 9 was inverted to obtain the vertical distributions of excited NO density $n^*(H)$ and kinetic temperature $T(H)$. The measured profile of band radiance is shown in Fig. 5. The points in this figure were obtained by removing the nonzero baseline and integrating the resulting spectra between $\lambda = 5.0838 \text{ } \mu\text{m}$ and $5.6370 \text{ } \mu\text{m}$. The noisy data above $H_T = 192 \text{ km}$ were replaced by the indicated exponential profile. The corrected and smoothed data were interpolated onto a uniform grid with intervals $\Delta H_T = 2.5 \text{ km}$ between $H_T = 100$ and 250 km . The integration mesh used to compute limb radiances extended to 400 km .

Two inversion results $n^*(H)$ are also shown in Fig. 5. Curve (a), which exhibits excessive vertical structure, was obtained by iterating until the rms relative difference between the observed and computed radiances was approximately one percent. This solution required 34 iterations. The other solution, continuous curve (b), represents an rms relative difference of 4.3 percent, and required six iterations. The result for five iterations (not shown) had a relative rms difference of 6.8 percent, and if plotted would be barely distinguishable from curve (b). The initial guess in each case was $n^*(H) = \text{const.} = 10^4 \text{ cm}^{-3}$.

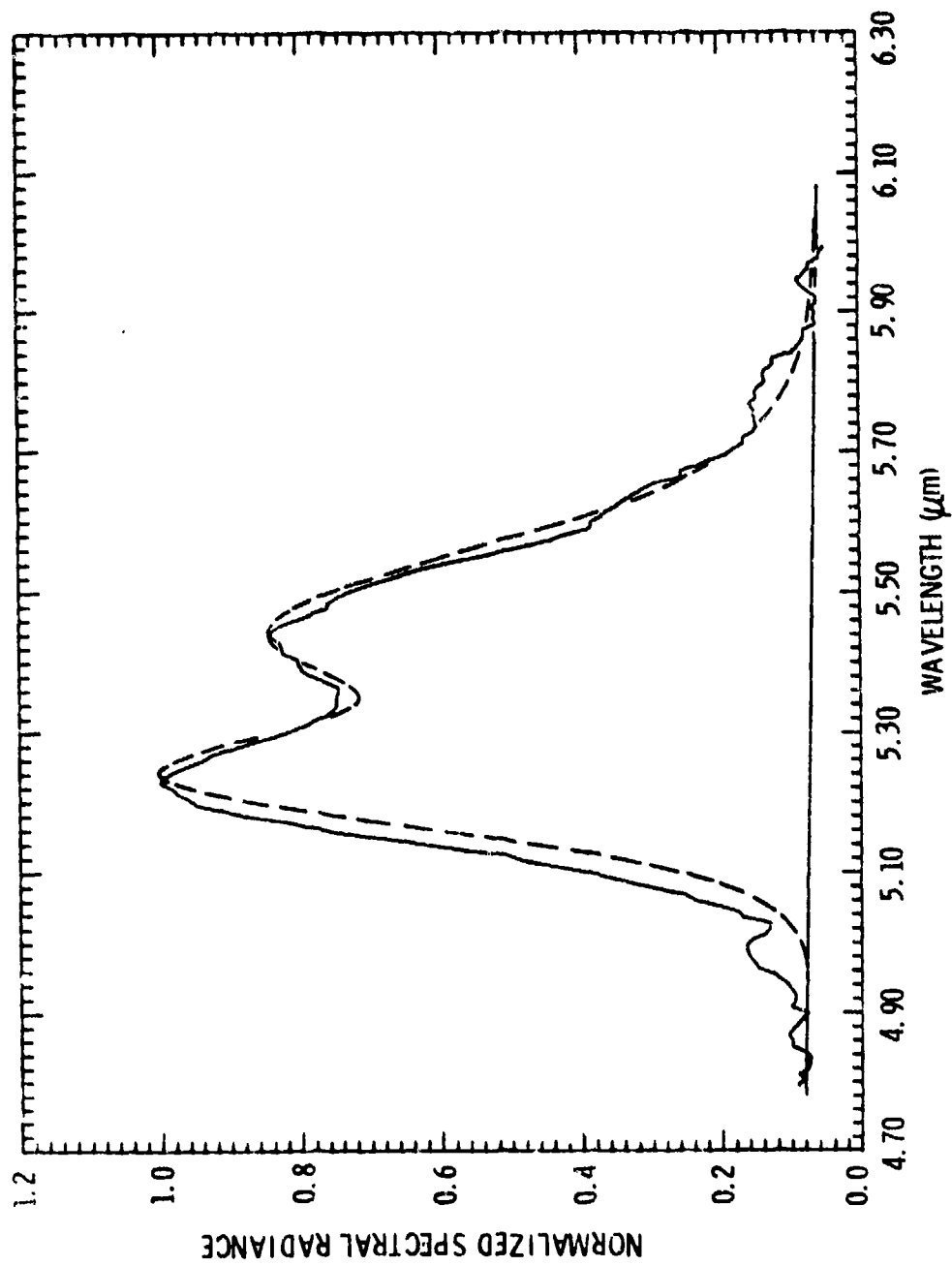


Figure 4. Spectral radiance measured by SPIRE at $H_T = 122$ km (continuous curve). The dashed curve is a computed spectrum described in Section 3.2.

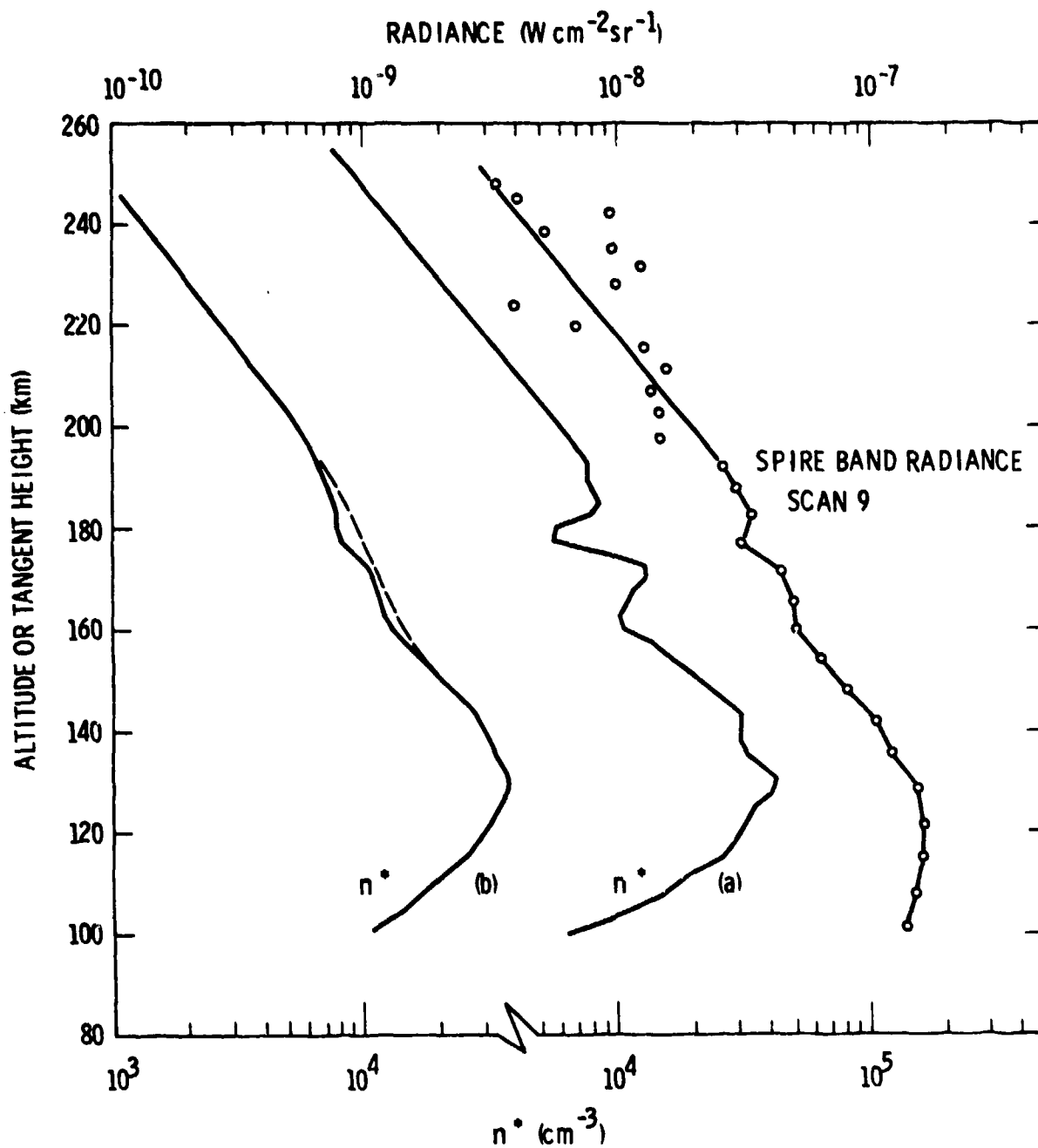


Figure 5. Corrected and smoothed NO limb radiance profile, and excited NO density profiles $n^*(H)$ obtained by inversion. The smoother solution (curve b) corresponds to a four-percent relative rms difference between observed and computed limb radiance profiles.

The sharp structure in solution (a) near 175 km is due to the sharp feature in the limb radiance profile near this altitude, which is probably a noise "spike". Note that the sensor, as it scans downward in tangent height, tends to produce a radiance profile that is roughly the integral of the $n^*(H)$ profile; that is, sharp features are integrated because of the sharp lower cutoff of the weighting function (Fig. 2). Thus, the solution can display unrealistic S-shaped features that resemble the derivative of noise spikes in the measured radiance profile. Solution (b) shows that noise has a smaller effect when the convergence criterion is set at a value that is closer to the expected rms relative noise in the measurements. For the purpose of deriving reaction rate constants and atmospheric cooling rates (Section 4), we used solution (b), but smoothed this result in the region of 170 km. The dashed curve in Fig. 5 represents the smoothed portion of the solution.

We found that the choice for the initial guess affected the rate of convergence, but had virtually no effect on the final solution.

3.2 Results for $T(H)$

Careful examination of the SPIRE spectral radiances and their variation with tangent height indicated that there were unknown shifts in the wavelength scale of the data. The shifts, which were in the range $\pm 0.03 \mu\text{m}$, appeared random with tangent height for some scans. We elected to use the SPIRE scan 9 data for the inversions because it had an apparent shift that was a relatively slow function of tangent height. The wavelength shifts were not large enough to seriously affect the band radiances calculated from the data.

The shifts were removed by the following procedure. A reference temperature profile, the solution $n^*(H)$ obtained from the scan 9 band radiances, and Eqs. (3b), (4) and (5) were used to compute a limb profile of spectral radiance $N(H_T, \lambda)$. The computed spectrum for $H_T = 122 \text{ km}$ (added to the baseline correction) is shown by the dashed curve in Fig. 4. The locations of the R and P branch maxima in the computed spectrum relative to those in the

measured spectrum were used to obtain the wavelength shift correction to the latter. We used the temperature profile given by the Jacchia (1977) model for an exospheric temperature 1050K (based on the U.S. Standard Atmosphere 1976) as the reference temperature profile.

After each of the measured spectra were shifted in this manner, a vertical temperature profile was recovered using the rotational temperature inversion procedure outlined in Section 2. It can be argued that the solution has been constrained by the necessity to assume a temperature profile in the correction of the unknown wavelength shifts. There is surely some measure of validity in this argument. However, noise in the spectral data probably had a much larger effect in the solution than the method used to correct for the shifts, and would probably have dominated even if no corrections had been made.

Figure 6 shows the SPIRE scan 9 measured spectral radiances for tangent heights of 148, 160 and 177 km. Because of the rapid deterioration of signal-to-noise above $H_T = 150$ km we made no attempt to recover the temperature above 150 km altitude. Also, the data used for the inversions was spectrally smoothed up to $H_T = 166$ km, and was discarded above this tangent height. We assumed that the spectral distribution of observed limb radiance remains constant for $H_T \geq 166$, and that the spectral radiances are proportional to the band radiance. This assumption implies constant temperature for $H \geq 166$, but should not have a large effect on the retrieved temperature profile below $H = 150$ km.

Some of the solutions $R[T(H_i), \lambda_k]$ obtained by inversion of the SPIRE data are shown in Fig. 7a. The ten selected wavelengths λ_k are 5.1, 5.15, 5.2, 5.25, 5.3, 5.35, 5.4, 5.5, 5.6 and 5.7 μm . Figure 7b shows theoretical $R(T, \lambda)$ values computed from Eq. (5) for various temperatures in the range 300K to 700K. The generally poor agreement between the set of recovered R's and computed R's is a result of the poor S/N of the spectral data, and possible wavelength scale "stretching" in the data.

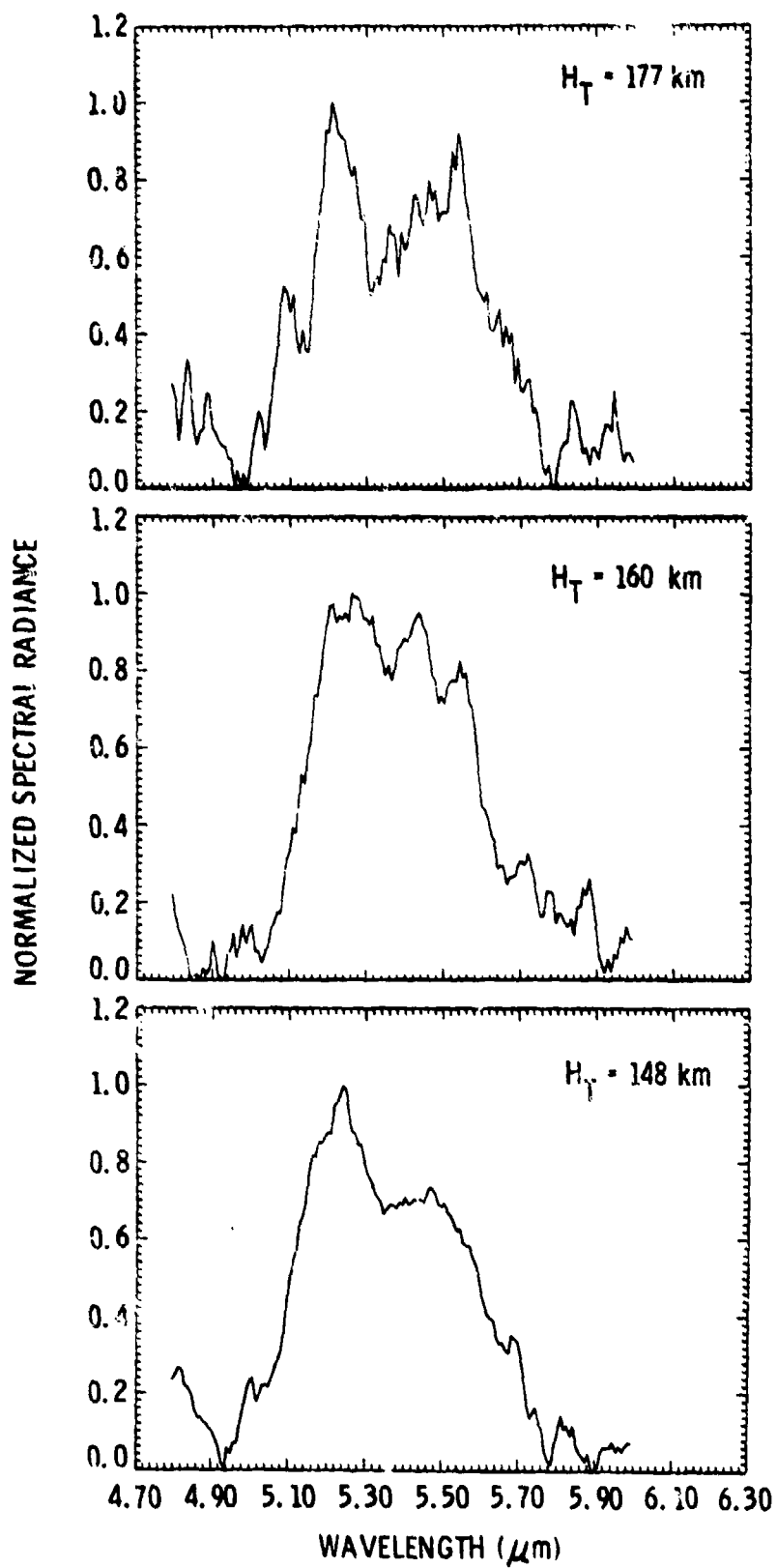


Figure 6. SPIRE spectral radiances for tangent heights of 148, 160 and 177 km. These spectra illustrate the rapid deterioration of signal-to-noise above $H_T \approx 150$ km.

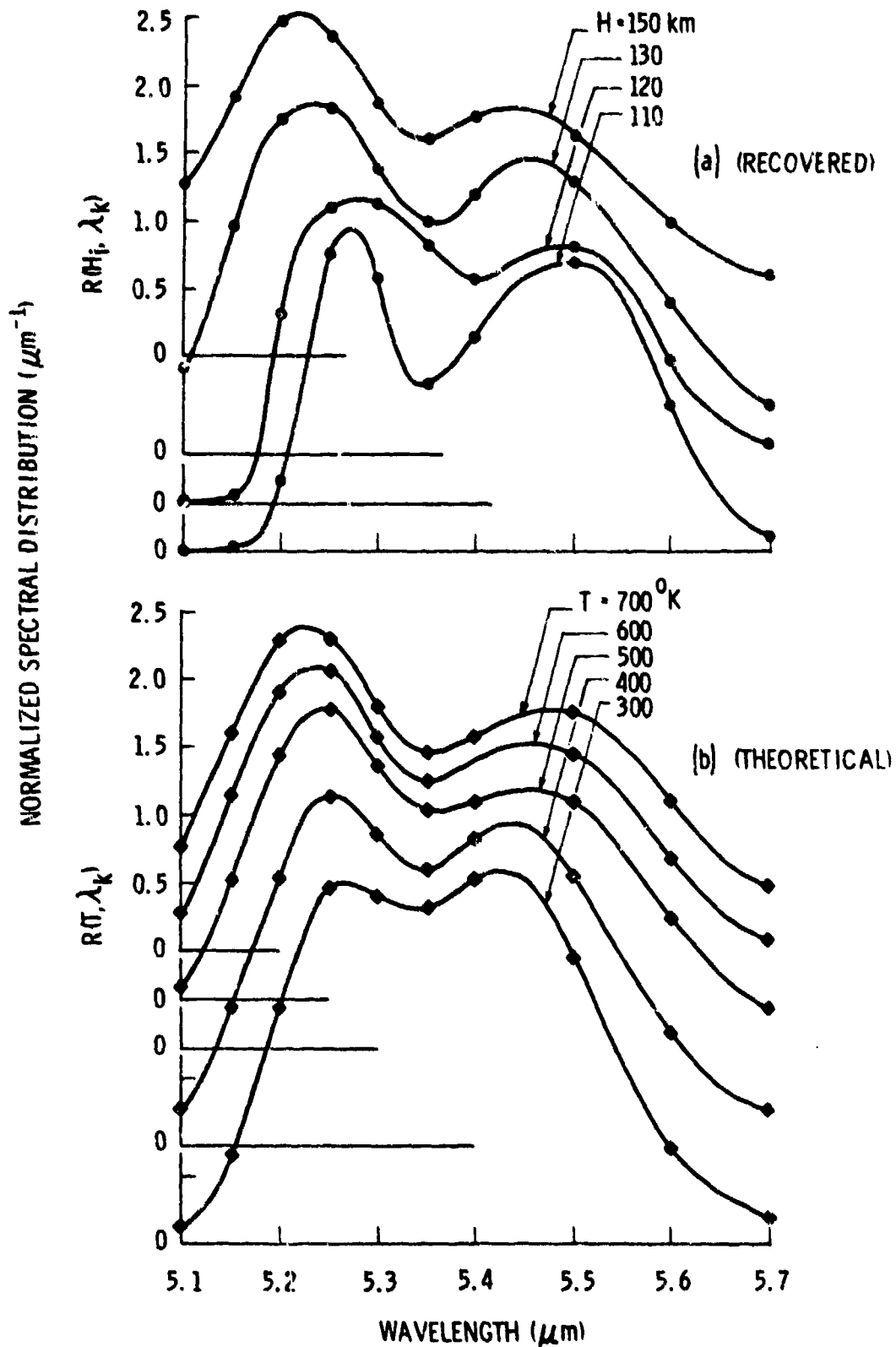


Figure 7. Some of the recovered spectral distributions $R[T(H_i), \lambda_k]$, and theoretical spectra $R(T, \lambda_k)$. R is the normalized apparent spectral emission per unit volume at rotational temperature T (see Eq. 5), and has units μm^{-1} .

Figure 8 shows the recovered temperature profile obtained by a systematic comparison of the solutions R_{ik} and a large library of computed $R(T, \lambda)$ spectra. Plotted in the same figure is the temperature profile given by the Jacchia model. The solution $T(h)$, although extremely noisy, is in rough agreement with the Jacchia profile above $H \simeq 120$ km. The S-shaped temperature excursions resemble those produced in the $n^*(h)$ solution by noise.

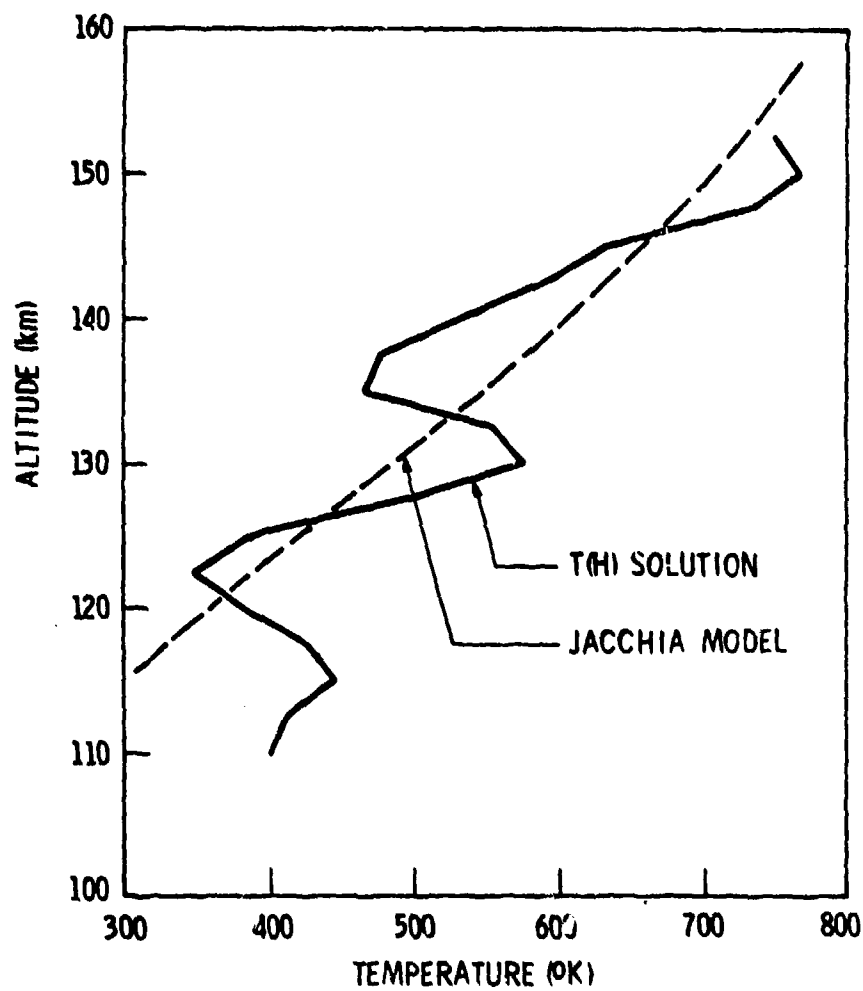


Figure 8. The temperature profile $T(H)$ obtained by inversion of the SPIRE NO spectral data, and a profile given by the Jacchia (1977) model.

SECTION 4
INTERPRETATION OF RESULTS

Kockarts (1980) pointed out that emission by the NO fundamental band is a major cause of heat loss in the upper atmosphere. He gives a simple formulation of the process, which results in a cooling rate L for the $5.3 \mu\text{m}$ band given by

$$L(H) = Ahc\tilde{\nu}n^*(H) \quad (13)$$

where h is Planck's constant, c is the velocity of light and $\tilde{\nu}$ is the wavenumber of the NO emission. ($Ahc\tilde{\nu} \approx 4.1 \times 10^{-12}$ if L has units $\text{erg cm}^{-3} \text{s}^{-1}$ and n^* has units cm^{-3}). The solution $n^*(H)$ obtained by inversion of the SPIRE data was used to calculate L . The result is compared in Fig. 9 to cooling rates given by Kockarts and by Gordiets *et al* (1980). The three results agree within a factor of four at $H = 120 \text{ km}$, and within a factor of two above 140 km . These differences are consistent with expected variations in n and n^* .

A steady state condition on the four important processes involving NO in the upper atmosphere (spontaneous emission by excited NO, excitation and deactivation of NO by collisions with O atoms, and excitation of NO through absorption of Earthshine) corresponds to the concentration ratio

$$\psi \equiv \frac{n^*}{n} = \frac{Ky + R}{\gamma + A} \quad (14)$$

where

n = the concentration of ground state NO,

$K = \exp(-hc\tilde{\nu}/kT) \approx \exp(-2698.5^\circ\text{K}/T)$,

γ = the rate of excitation of NO due to O atoms,

A = the Einstein emission coefficient = 10.78 s^{-1} ,

R = the rate of production of excited NO due to absorption of Earthshine;

$R = \pi B_\nu S$ where

$B_\nu(T_E)$ = the Planck spectral emission rate corresponding to the effective Earthshine temperature T_E , and

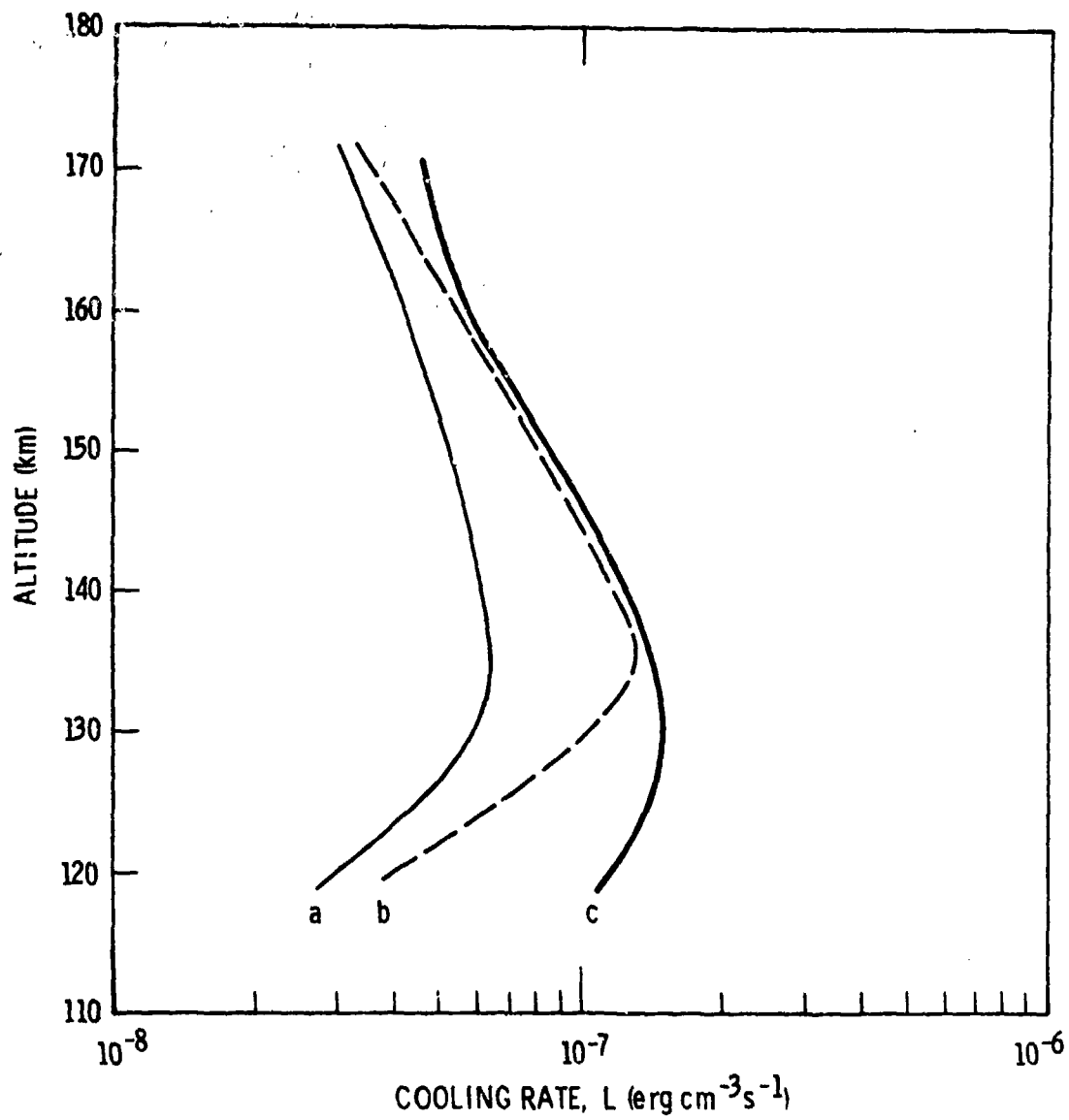


Figure 9. Comparison of cooling rates given by Gordiets *et al* 1980 (curve a), by Kockarts 1980 (curve b), and obtained from the inversion solution $n^*(H)$ (curve c).

S = the band strength of the $5.3 \mu\text{m}$ band $\approx 503 \times 10^{-20}$ cm/molec at 296K (Rothman *et al* 1981).

The excited concentration n^* is known from inversion of the SPIRE NO data. If models are adopted for $n(H)$ and $T(H)$, then we know $\psi(H)$ and $K(H)$, and can solve Eq. (14) for $\gamma(H)$:

$$\gamma(H) = (A\psi - R)/(\psi - K) \quad (15)$$

Over the altitude range for which Eq. (15) will be evaluated, R can be neglected in comparison to $A\psi$. The de-excitation rate constant k_0 for the reaction



can be obtained from $\gamma(H) = k_0[O]$ if a model is also adopted for the concentration of oxygen atoms $[O(H)]$.

Table 1 shows the results of the calculation of k_0 . The kinetic temperature profile is the one given by the Jacchia (1977) model, as described earlier. The distribution $n(H) \equiv [\text{NO}(H)]$ is the "median" model suggested by Caledonia *et al* (1980), and the profile for $[O]$ is taken from Jacchia (1977).

The average of k_0 over the altitude range 130-160 km is $\sim 7.8 \times 10^{-11} \text{ cm}^{-3} \text{ s}^{-1}$, which compares favorably with the value 6.5×10^{-11} measured by Fernando and Smith (1979) at a temperature of 300K. Glazer and Troe (1975) measured the value $3.6 \times 10^{-11} \text{ cm}^{-3} \text{ s}^{-1}$ at 2700K. If we use the "auroral" model for $[\text{NO}]$ given by Caledonia *et al* (1980), which has NO concentrations approximately five times higher than the "median" model, we obtain an average k_0 value of $1.4 \times 10^{-11} \text{ cm}^{-3} \text{ s}^{-1}$.

Table 1. De-excitation rate constant k_0 for reaction $\text{NO}^* + \text{O} \rightarrow \text{NO} + \text{O}$

H (km)	T (°K)	n^* (cm^{-3})	$n \equiv [\text{NO}]$ (cm^{-3})	$[\text{O}]$ (cm^{-3})	k_0 ($\text{cm}^{-3}\text{s}^{-1}$)
130	491	3.7×10^4	3.3×10^7	4.8×10^{10}	8.2×10^{-11}
140	609	3.0(4)	1.8(7)	2.9(10)	6.2(-11)
150	707	2.1(4)	9.0(6)	1.8(10)	7.0(-11)
160	785	1.4(4)	4.5(6)	1.2(10)	9.6(-11)

REFERENCES

- Ahmadjian, M., Smith, D.R. and Stair, A.T. Jr. 1981, "COIRIS -- A Cryogenic Infrared (IR) Radiance Instrument for Shuttle," Proc. Soc. Photo-Opt. Instr. Eng., 280, 45.
- Billingsley, F. 1975, "Calculated Vibration-Rotation Intensities and Line Positions for Ground State Nitric Oxide," TR-75-0586, Air Force Geophysics Laboratory, Hanscom AFB, MA.
- Caledonia, G. *et al.* 1980, "COCHISE Research," Physical Sciences, Inc., TR-233.
- Fernando, R. and Smith, I. 1979, "Vibrational Relaxation of NO by Atomic Oxygen," Chem. Phys. Letters, 66, 218.
- Gille, J.C. and House, F.B. 1971, "On the Inversion of Limb Radiance Measurements I: Temperature and Thickness," J. Atmos. Sci., 28, 1427.
- Glazer, K. and Troe, J. 1975, "Vibrational Relaxation of NO in Collisions with Atomic Oxygen and Chlorine," J. Chem. Phys., 63, 4352.
- Gordiets, *et al.* 1980, "The Influence of Radiative Cooling and Turbulence on the Heat Budget of the Thermosphere," 23rd COSPAR Symposium, Budapest, Hungary.
- Halem, M. and Chow, M. 1976, "Sounder Design Considerations in the Selection of Temperature Sensing Channels," J. Appl. Met., 15, 394.
- Jacchia, L. 1977, "Thermospheric Temperature, Density and Composition: New Models," Smithsonian Astrophysical Observatory, Special Report 375.
- Kockarts, G. 1980, "Nitric Oxide Cooling in the Terrestrial Thermosphere," Geophys. Res. Letters, 7, 137.
- Nadile, R.M., *et al.* 1977, "SPIRE -- Spectral Infrared Experiment," Proc. Soc. Photo-Opt. Instr. Eng., 124, 118.

Rothman, L. S., *et al.* 1981, "AFGL Trace Gas Compilation: 1980 Version,"
Appl. Opt., 20, 1323.

Stair, A.T. Jr., *et al.* 1981, "Infrared Measurements of Aurora, Airglow and
the Upper Atmosphere," AIAA 19th Aerospace Sciences Meeting,
January 12-15, 1981, St. Louis, Missouri (AIAA-81-0421).

APPENDIX A
ANALYTICAL SOLUTIONS FOR EXPONENTIAL n^* OR n^{**}

The integral in Eq. (2) can be evaluated in terms of the modified Bessel function of the second kind when $n^*(H)$ is exponential. One can show that the Bessel function reduces to an exponential if certain geometrical approximations are made. We will derive this exponential solution starting directly from the geometrical approximations.

The partial derivative in Eq. (2) is given by (see Fig. 1a)

$$\begin{aligned} \partial z(H, H_T) / \partial H &= (R+H) [(R+H)^2 - (R+H_T)^2]^{-1/2} \\ &\approx (R/2)^{1/2} (H - H_T)^{-1/2} \end{aligned} \quad (A-1)$$

where the second form results from expanding the terms in the radical and neglecting H and H_T compared to R , the Earth's radius. With this approximation and assuming the distribution

$$n^*(H) = n_0^* \exp[-(H - H_0)/H_S] \quad (A-2)$$

we can write Eq. (2) in the form

$$N(H_T) \approx \frac{2A}{4\pi} \left(\frac{R}{c}\right)^{1/2} n_0^* e^{-(H_T - H_0)/H_S} \int_0^\infty \frac{e^{-x/H_S}}{x^{1/2}} dx. \quad (A-3)$$

The definite integral is equal to $\sqrt{\pi H_S}$; hence

$$\begin{aligned} N(H_T) &\approx (2A/4\pi) (\pi R H_S / 2)^{1/2} n_0^* \exp[-(H_T - H_0)/H_S] \\ &= (2A/4\pi) (\pi R H_S / 2)^{1/2} n^*(H_T). \end{aligned} \quad (A-4)$$

The contribution of an Earth-concentric layer (H_1, H_2) to the radiance observed at tangent height H_T is obtained by generalizing the integration limits in Eq. (A-3):

$$N(H_T, H_1, H_2) \approx \frac{2A}{4\pi} \left(\frac{R}{2}\right)^{1/2} n_0^* e^{-(H_T - H_0)/H_S} \int_{H_1}^{H_2} \frac{e^{-(H-H_T)/H_S}}{(H-H_T)^{1/2}} dH . \quad (A-5)$$

This result can be expressed in terms of $n^*(H_T)$ and the error function:

$$\begin{aligned} N(H_T, H_1, H_2) &= (2A/4\pi) (\pi R H_S / 2)^{1/2} n^*(H_T) \\ &\times \left[\operatorname{erf} \left\{ [(H_2 - H_T)/H_S]^{1/2} \right\} - \operatorname{erf} \left\{ [(H_1 - H_T)/H_S]^{1/2} \right\} \right] ; \\ &H_1 \geq H_T . \end{aligned} \quad (A-6)$$

The limb profile given by Eq. (A-4) or (A-6) must be convolved with the sensor field of view function to obtain the observed limb radiance profile, unless n^* varies by a relatively small amount over the vertical distance resolved by the sensor.

APPENDIX B
INVERSION USING FOURIER TRANSFORMS

The predicted limb radiance profile for the *optically-thin case* is obtained by evaluating Eq. (2) and convolving the result $N(H_T)$ with the sensor IFOV function $I(H_T)$. If the geometric approximation represented by Eq. (A-1) is used in evaluating $N(H_T)$, the predicted or observed limb radiance profile can be expressed as

$$\tilde{N}(H_T) \approx I(H_T) * (2A/4\pi)(R/2)^{1/2} \int_{H_T}^{\infty} dH \cdot (H-H_T)^{-1/2} n^*(H) \quad (B-1)$$

The integral in Eq. (B-1) is another convolution; thus,

$$\tilde{N}(H_T) \approx B \cdot I * W * n^* \quad (B-2)$$

where

$$B = \text{const.} = (2A/4\pi)(R/2)^{1/2}$$

and

$$W = \begin{cases} (-H)^{-1/2} & \text{for } H \leq 0 \\ 0 & \text{otherwise} \end{cases} \quad (B-3)$$

By the convolution theorem, Eq. (B-2) has the Fourier transform

$$F(\tilde{N}) \approx BF(I*W)F(n^*) \quad (B-4)$$

where $F(\)$ denotes a Fourier transform; likewise, $F^{-1}(\)$ will denote the inverse Fourier transform. The desired inversion solution $n^*(H)$ can be obtained as

$$n^*(H) \approx F^{-1} \left\{ F(\tilde{N}) / [BF(I*W)] \right\} \quad (B-5)$$

The effective weighting function $I*W$ is finite everywhere and can be truncated (and apodized), since $n^* = 0$ above some high altitude. Hence,

its Fourier transform exists and can be evaluated once and for all.* Therefore, the routine evaluation of Eq. (B-5) for a given sensor involves only two Fourier transforms, which can be performed using the Fast Fourier Transform (FFT) method, and one intermediate division (multiplication). Note that $F(I*W)$, and hence $F(\tilde{N})$, can have zeroes at some spatial frequencies. This will make n^* the transform of a function that is indeterminate at some frequencies, but it is likely that the indeterminacies can be resolved by interpolation.

We emphasize that this method of limb radiance inversion is untested and restricted to the optically-thin case.

*Note that $F(W)$ does not exist.